

Equilibrium behaviour of a novel gas separation process, with application to carbon capture

M. B. Sweatman

Department of Chemical and Process Engineering, University of Strathclyde, Glasgow, UK. G1 1XJ

A novel 'pressure-swing wetting layer absorption' gas separation process is described and analysed in the context of carbon capture. This work examines the equilibrium behaviour of this process using the density functional theory (DFT) of classical fluids. Under the conditions investigated here we find that the equilibrium behaviour of this system is superior to the analogous pressure-swing adsorption process without solvent. However, further experimental and process modelling work is needed to confirm this. (*Chem. Eng. Sci.* **65**, p3907 (2010))

1. Pressure-swing wetting layer absorption – the basic process

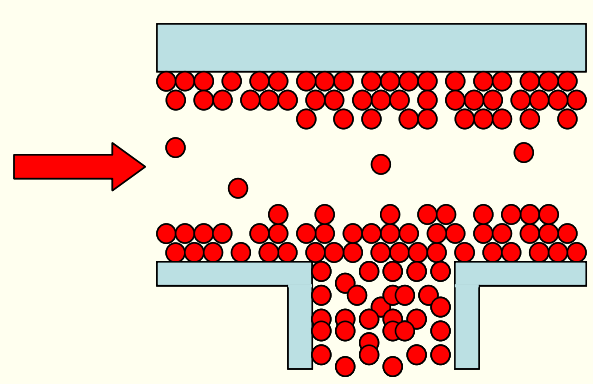


Figure 1a. The physical absorbent fluid (red) is premixed as a vapour with the gas mixture to be separated and adsorbed into a porous material. Narrow pores fill with absorbent fluid while wider pores remain empty. This effectively creates a very high surface area vapour liquid interfacial area, many orders of magnitude higher than in an adsorption column.

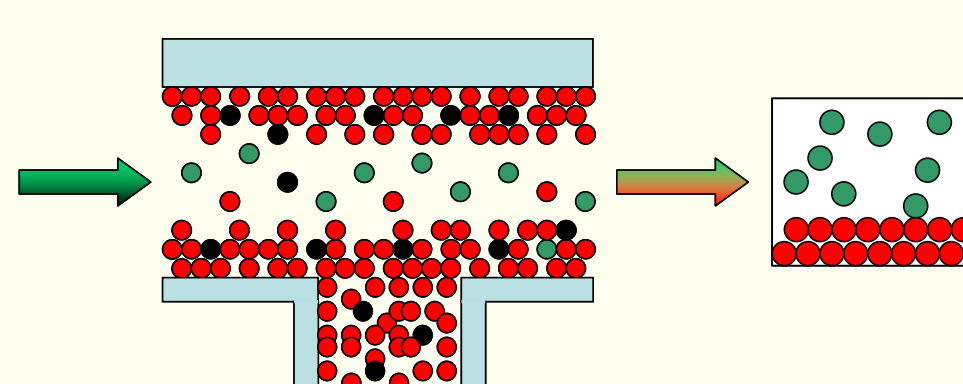


Figure 1b. In the first part of the pressure swing absorption cycle the gas to be separated is passed through the combined porous material – absorbent fluid system. The gas component to be separated (black) is strongly absorbed into the absorbent fluid. The other gas component (green) is weakly absorbed, and mostly passes through the absorption chamber.

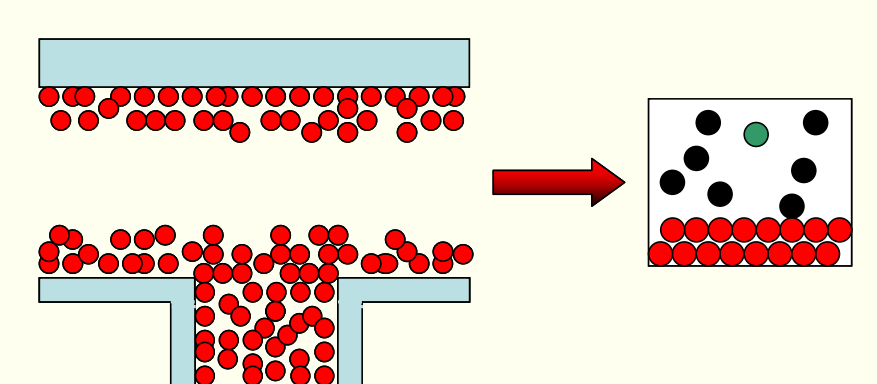


Figure 1c. The second stage of the process recovers the absorbed gas, as well as some of the absorbent fluid, by reducing the pressure. Due to the extremely high interfacial area the process could be more compact and efficient than traditional absorption columns, and more selective than standard adsorption processes.

2. Results: capacity and selectivity of CO₂ based on a DFT model of THF solvent in carbon slit-pores

A classical density functional theory (DFT) model of the *equilibrium* behaviour of the process was developed, i.e. it is assumed that the entire adsorption/absorption bed is in equilibrium with the exhaust gas.

THF (tetrahydrofuran) is chosen as the physical absorbent (solvent) while the adsorbent (which is taken to be an activated carbon) is modelled in terms of ideal graphitic slit-pores. The exhaust gas is modelled as a mixture of CO₂ and N₂, with CO₂ mole fraction of 0.1, total pressure of 1 bar, and temperature of 298 K.

A range of pore widths, denoted H , and solvent partial pressures have been studied. Results for the Capacity and Selectivity of CO₂ are obtained. Capacity simply measures the ratio of the density of CO₂ within the pore compared to the bulk density, i.e. It measures the amount of gas that can be processed. So,

$$C_{CO_2} = \frac{1}{H\rho_{b,CO_2}} \int_0^H dz \rho_{CO_2}(z)$$

where ρ is the density, z is the distance across the slit-pore, and the b subscript indicates the bulk value. The selectivity of CO₂ is defined here simply as $S_{CO_2} = C_{CO_2} / C_{N_2}$.

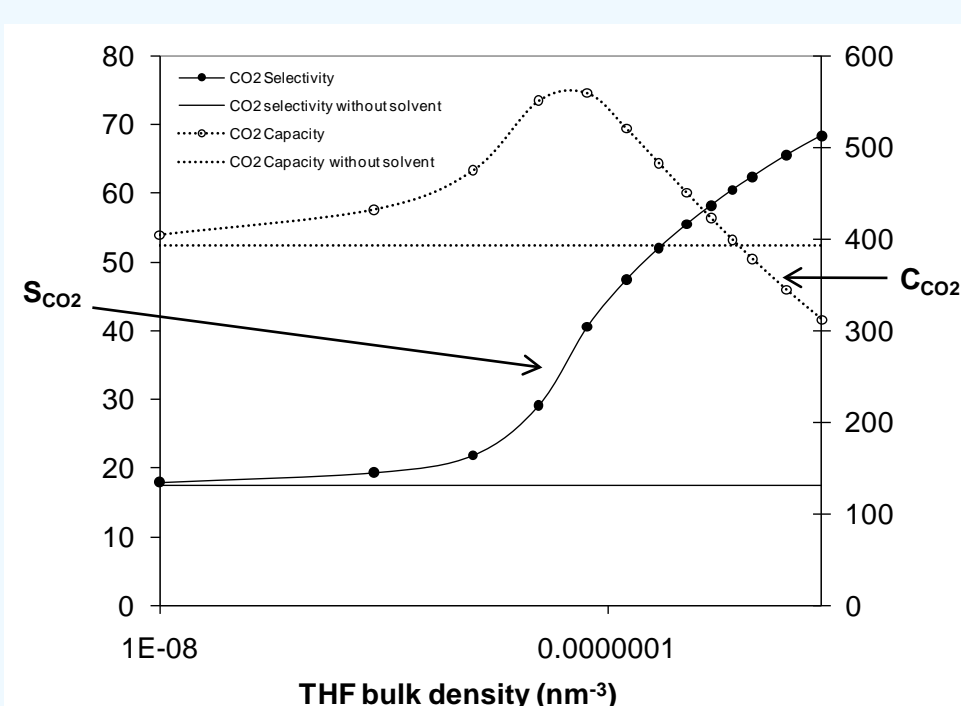


Figure 2a. DFT model predictions for a model 0.8 nm graphitic pore. Symbols indicate actual calculations while the curved lines are simply a guide to the eye. The horizontal lines correspond to results without THF, i.e. for the analogous pressure-swing adsorption process. Note how for bulk densities $\sim 1 \times 10^{-7} \text{ nm}^{-3}$ the selectivity is more than twice that of the standard adsorption process, while the capacity is very similar.

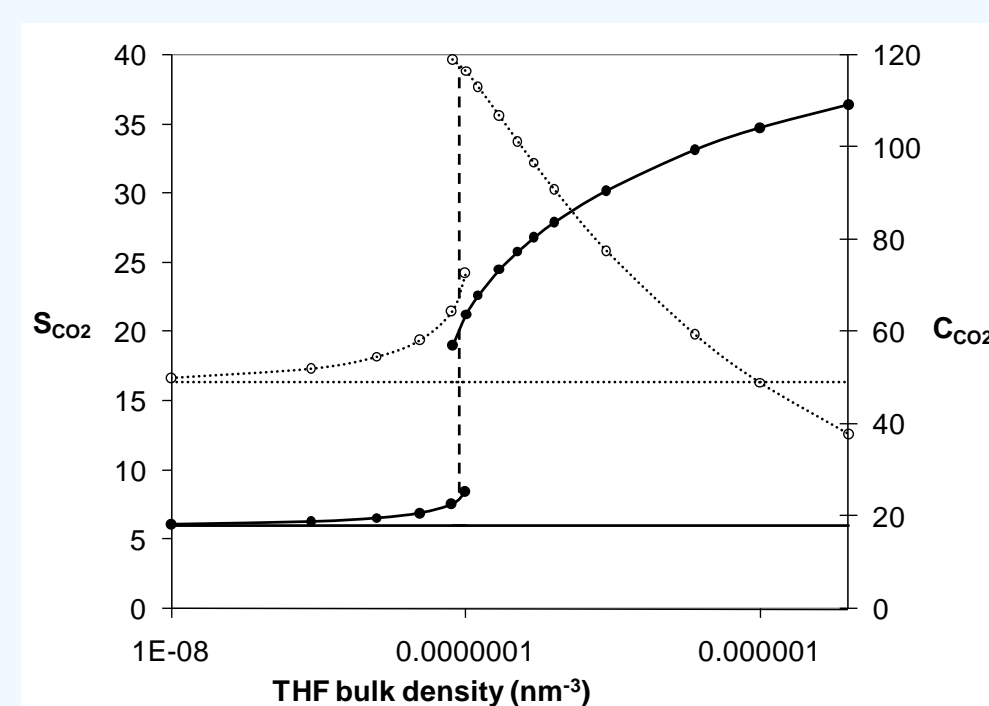


Figure 2b. As for Figure 2a, except that the pore is 1.0 nm wide. There is now a pore-filling phase transition at $1 \times 10^{-7} \text{ nm}^{-3}$ indicated by the vertical dotted line. Note how both the selectivity and capacity are both much higher than for the standard adsorption process just after the pore filling transition.

SUMMARY: for an active carbon with predominantly $\sim 1 \text{ nm}$ pores the wetting layer absorption process could have greater selectivity and capacity than the standard adsorption process under the same conditions.

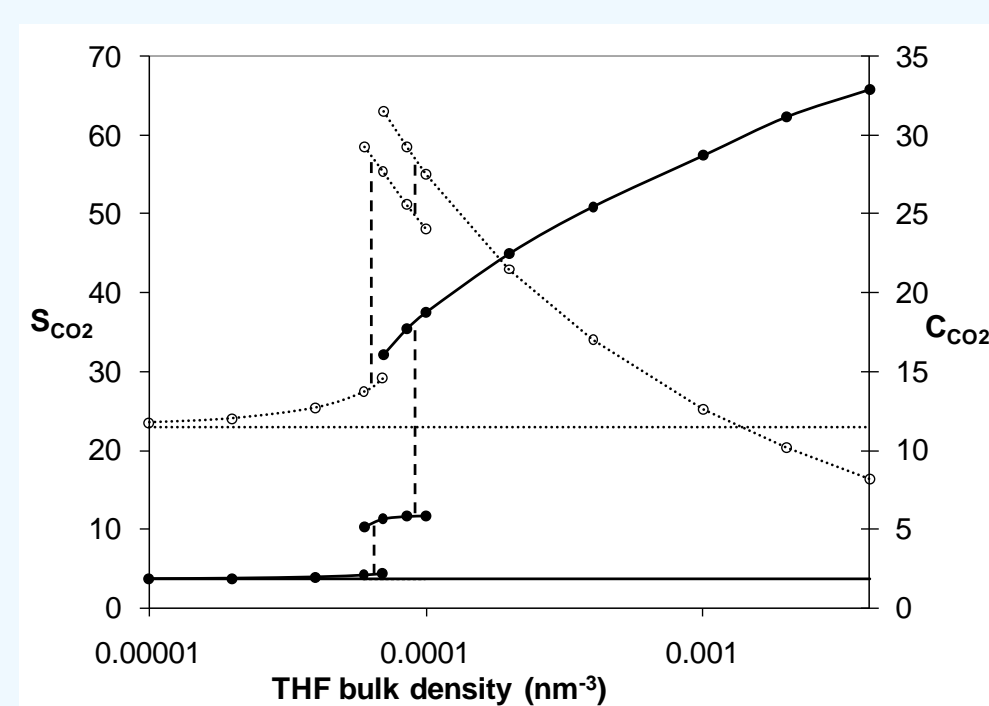


Figure 2c. As for Figure 2a, except that the pore is 2.0 nm wide. There is now a monolayer phase transition at $\sim 9 \times 10^{-5} \text{ nm}^{-3}$ and capillary condensation at $\sim 1 \times 10^{-5} \text{ nm}^{-3}$. Once again, both the selectivity and capacity are both higher than for the standard adsorption process just after the pore filling transition.

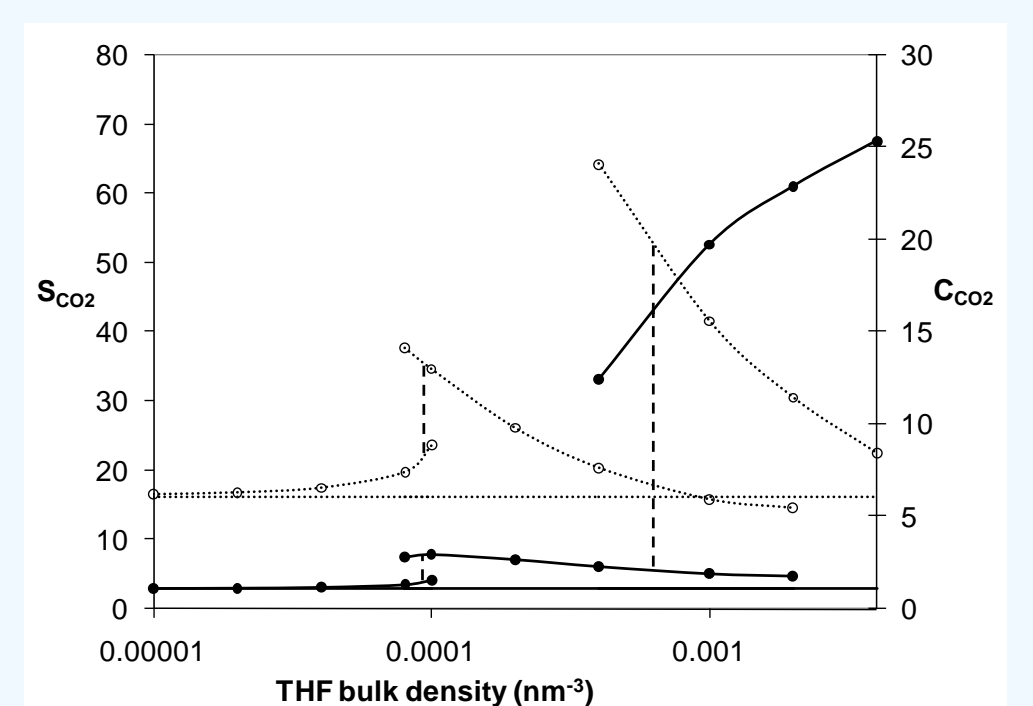


Figure 2d. As for Figure 2a, except that the pore is 4.0 nm. There is now a monolayer phase transition at $\sim 1 \times 10^{-3} \text{ nm}^{-3}$ and capillary condensation at $\sim 9 \times 10^{-3} \text{ nm}^{-3}$. Once again, both the selectivity and capacity are both higher than for the standard adsorption process just after the pore filling transition. Notice how the capacity drops quickly with increasing pore width, while the selectivity does not.

3. CO₂ recovery

CO₂ can be recovered by reducing the pressure. Of course, nitrogen and some THF will also be recovered. The same DFT model is used to model this process as in Section 2. Once again, it is assumed that the entire adsorption/absorption bed is in equilibrium with the bulk gas phase. The amount of each gas component desorbed during an incremental drop in pressure is taken to be proportional to the bulk density of each gas component, because it is gas in the bulk phase that is extracted from the adsorption/absorption chamber.

To determine a desorption profile it is first necessary to define a distribution of pore sizes. For simplicity, in this work the porous material is taken to consist of equal volumes of 0.8 nm and 4.0 nm pores. This kind of bimodal pore size distribution is actually quite reasonable. For instance, a carbon xerogel¹ formed by aggregation of active carbon nanoparticles via a sol-gel process could have a distribution of pore sizes similar to this. For this combination of pores a sensible THF bulk density is $1 \times 10^{-7} \text{ nm}^{-3}$. The same initial bulk gas composition is used as in the previous section, corresponding to a total pressure of 1.0 bar.

Figure 3 compares the recovery of CO₂ for the wetting layer absorption process and the analogous adsorption process. Results are shown for the total number of molecules of each gas recovered per square nanometer of pore area during desorption from 1.004 bar to low pressure (0.0103 bar). To begin with, as pressure is reduced, nitrogen, being the most volatile component, is recovered. Eventually, at around 0.1 bar, nitrogen is mostly depleted from the chamber and the rate of CO₂ recovery with reducing pressure increases dramatically for both processes. However, about 3 times as much nitrogen is recovered with the standard adsorption process, so the wetting layer absorption process is much more effective.

CONCLUSION: the wetting layer absorption process could be much more efficient than a standard adsorption process under the same conditions. However, this analysis ignores very important non-equilibrium effects, such as heat and mass transport, and so experiments and process simulations are needed to investigate further.

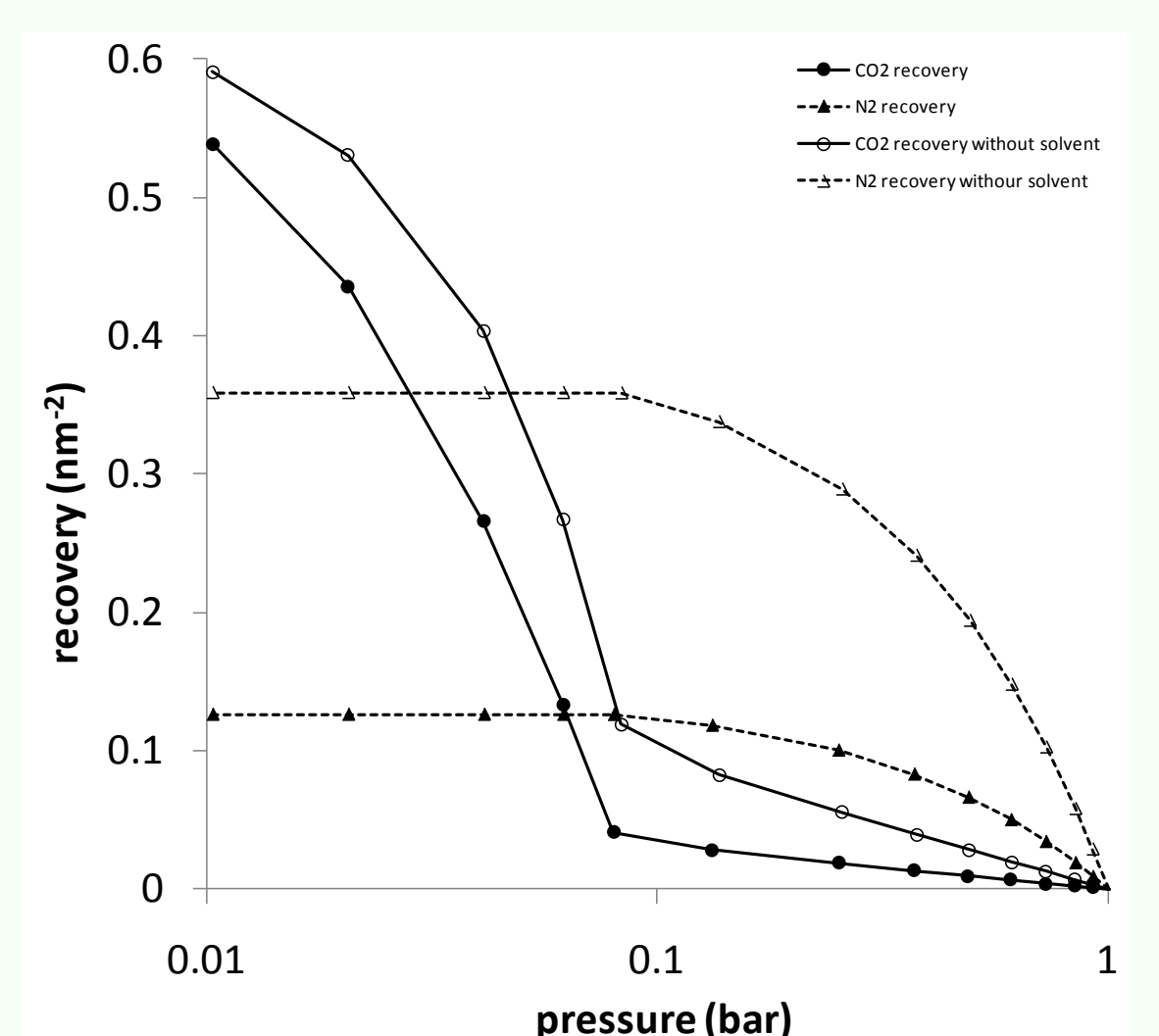


Figure 3